Spatial Resolution of the Pressure Anemometer

W. A. OOST AND G. J. KOMEN

Royal Netherlands Meteorological Institute (KNMI), Wilhelminalaan 10, 3730 AE De Bilt, Netherlands

(Manuscript received 19 January 1983, in final form 5 July 1983)

ABSTRACT

One of the important characteristics of an anemometer is its spatial resolution. A three-dimensional generalization is given of a method to calculate the transfer function as a function of the wavenumber, devised by Kaimal *et al.* for a sonic anemometer. The method has been applied to the sensor system of the pressure anemometer, a new type of wind vector measuring instrument. The results, given in a number of figures, show an extremum before the transfer function falls off to its final value.

1. Introduction

One of the important characteristics of an anemometer is its useful frequency response. Two factors can be distinguished: 1) the intrinsic frequency response, determined by the speed with which various elements in the instrument react to a change in windspeed and 2) the limitations on the useful frequency range due to the finite dimensions of the wind sensing system.

The second factor, which is in fact a wavelength effect, is the subject of this paper. The calculations are a generalization of a method outlined by Kaimal *et al.* (1968) and Horst (1973), which is based on earlier work by Uberoi and Kovasznay (1953), Gurvich (1962) and Silverman (1968).

Kaimal *et al.* and Horst developed their method for a three-dimensional sonic anemometer with the well-known nonorthogonal sensor configuration (Fox, 1968); they could treat the vertical component of the sensor separately from the two horizontal ones. For the pressure anemometer, which is the subject of this paper, this is not possible. A pressure anemometer (PA) is in principle a combination of six pressure tubes, arranged in three mutually orthogonal sets of two. The two tubes in each set are pointing in opposite directions and connected to the ports of a differential pressure transducer. From the readings of the three transducers the wind velocity and direction can be derived. To keep the tubes clean inside, a continuous airflow is forced through the tubes from within the instrument. The tubes are, in reality, not tubes but chambers in a hollow ring, split into two compartments by a partition which lies in the centerplane of the ring. The outlet port of a "tube" consists of four openings on one side of a ring, distributed evenly along that ring. Each ring contains both tubes of a set, so there are eight holes in each ring, four on each side. For a full description of the instrument, see Oost (1983).

The full sensor system of the PA consists of three rings with mutually orthogonal axes tilted so that these axes all have the same angle toward the horizontal plane. This angle, as can be easily calculated, is $\cos^{-1}(2/3)^{1/2}$ or $\sim 35.26°$. The situation is depicted in Fig. 1; the dashed line is along the vertical when the instrument is in an upright position.

There are, of course, an infinite number of configurations that fit the description; when the rings are displaced parallel to their own plane they stay mutually orthogonal and the angle with the horizontal plane is conserved. The configuration of Fig. 1 was chosen to minimize the mutual distance of the sensor rings for a given length from M to the center of the rings. If the rings are displaced in the way as indicated by the arrows near M, another interesting configuration is obtained, viz. of minimum mutual interference in the wind. The wind is sensed by a set of four pairs of holes on each ring.

To prevent semantic problems, the terms "component" and "sensor", as far as they will be applied to instruments, are defined as

- A component is a part of the sensor system that functions more or less independently and measures—at least to some degree of approximation —one component of the windvector.
- A sensor is a subsystem of a component, that contributes part of its signal.

For the PA, a ring is a component and each opening on the ring is a sensor.

The finite dimensions of the sensing system are the cause of several types of frequency response degradation: 1) due to the dimensions of the sensors, 2) due to the spatial separation of the sensors on one com-

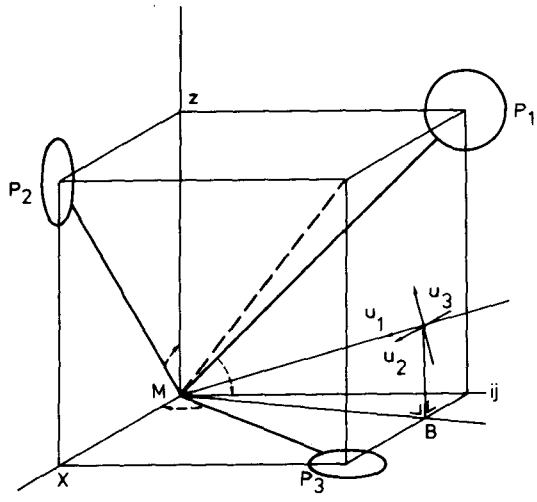

FIG. 1. Coordinate systems of the pressure anemometer (x, y, z) and the wind (u_1, u_2, u_3). The u_1 component is along the mean wind, u_2 is perpendicular to u_1 and parallel to the xy-plane and u_3 is perpendicular to u_1 and u_2. The dashed line is along the vertical, so the plane of P_1, P_2 and P_3 is horizontal. The ring with its center at P_1 is sensitive to the windcomponent in the x-direction only, those at P_2 and P_3 to the y- and z-component, respectively. The direction of the mean wind in this figure is very unusual (an elevation of about 60°) and was chosen only for graphical reasons.

ponent, and 3) due to the distances between the components.

The first type is very important, e.g., a sonic anemometer, where the dimension meant is the distance between a transmitter and a receiver, but with the PA it is the diameter of a sensor opening, which is less than 1 mm, and therefore negligible. Deviations of the second type are considered to be nonnegligible for the PA (although those of the third type are dominant). There are two lengths in this connection—the distance between two neighboring openings on one side of a ring and between two openings on different sides of that ring. The first one is of the order of 23, the other of 5 mm; both are retained in the calculations.

The third type of deviation has been treated by Kaimal *et al.* (1968) for a two-dimensional nonorthogonal system. In their case this was sufficient, as the midpoint of the vertical component of the sonic coincided with that of the line connecting the midpoints of the other two components. For the PA this simplification cannot be used, due to the different geometry and the fact that the signals are treated as a set, so a three-dimensional treatment is necessary. As a kind of compensation for the added complexity, the components of the PA are mutually orthogonal.

Two effects will be neglected that are related to those treated: the differences in the contributions of individual sensors to the signal of a component and time of travel effects in a component, due to the different distances of the various sensors to the pressure transducer that transforms the pressure signal for a component into an electric signal. The first effect has been neglected because we have no reliable data on it, although there are indications that it does exist. The second effect can indeed be neglected, because the pressure waves from the sensor openings travel at the speed of sound. A distance of 2 cm between the openings gives a difference in time of arrival at the pressure transducer of less than 0.1 m s. This is well outside the frequency range of the PA because the intrinsic frequency response of the instrument has its 3 dB point at ~35 Hz (Oost, 1983).

2. Method

We will follow the method outlined by Kaimal *et al.* (1968), which can be summarized as follows:

The three-dimensional wind field $\mathbf{u}(\mathbf{x}, t)$ with $\mathbf{x}$ the space and t the time coordinate, is assumed to be homogeneous, isotropic and stationary. Each component of the turbulent velocity field $u_l(\mathbf{x})$ can be expanded as a Fourier-Stieltjes integral (see, e.g., Lumley and Panofsky, 1964, p. 16)

$$u_l(\mathbf{x}) = \int_{-\infty}^{+\infty} \exp(i\mathbf{k}\cdot\mathbf{x})dU_l(\mathbf{k}), \tag{1}$$

with $\mathbf{k}$ the wavenumber vector. The time coordinate has been omitted because of the supposed stationarity. The $U_l(\mathbf{k})$ are random functions with orthogonal increments which are used to define the spectral density tensor $\Phi_{ln}(\mathbf{k})$

$$\overline{dU_l(\mathbf{k})[dU_n(\mathbf{k}')]^*} = \Phi_{ln}(\mathbf{k})d\mathbf{k}\delta(\mathbf{k}' - \mathbf{k}), \tag{2}$$

where an asterisk denotes a complex conjugate, an overbar an ensemble average and $\delta(\mathbf{k}' - \mathbf{k})$ is the Dirac delta function, the use of which is a consequence of the homogeneity. We will further assume that the relevant wavenumbers lie in the inertial subrange (Lumley and Panofsky 1964, p. 29) so

$$\Phi_{ln}(\mathbf{k}) = \frac{\epsilon^{2/3}}{4\pi} k^{-17/3}(k^2\delta_{ln} - k_l k_n). \tag{3}$$

Here ϵ is the turbulent energy dissipation, δ_{ln} the Kronecker delta and $k = |\mathbf{k}|$. The relation between $\Phi_{ln}(\mathbf{k})$ and the components of the velocity field is

$$R_{ln}(\mathbf{r}) = \overline{u_l(\mathbf{x})u_n(\mathbf{x}+\mathbf{r})} = \iiint_{-\infty}^{+\infty} \exp(i\mathbf{k}\cdot\mathbf{r})\Phi_{ln}(\mathbf{k})d\mathbf{k}, \tag{4}$$

which is independent of Φ due to the homogeneity assumption.

In practice, however, spatial correlations cannot be measured. The quantity presented as the spectrum is obtained by analyzing the fluctuations in time, mea-

sured by a single fixed instrument, so it is basically a frequency spectrum in the direction of the mean wind (X_1 direction). With the use of the Taylor hypothesis this frequency spectrum can be transformed into a one-dimensional wavenumber spectrum in the X_1-direction, which will be indicated as $F_{ln}(k_1)$ giving

$$R_{ln}(r_1, 0, 0) = \overline{u_l(\mathbf{x})u_n(\mathbf{x} + \mathbf{r}_1)} = \int_{-\infty}^{+\infty} \exp(ik_1 r_1) F_{ln}(k_1) dk_1, \quad (5)$$

where $r_1 = u_1 t$, with u_1 the mean velocity in the $\mathbf{X}_1$-direction and t the time interval; (5) is again independent of $\mathbf{X}$ due to the homogeneity. Comparing (4) and (5) it is clear that

$$F_{ln}(k_1) = \iint_{-\infty}^{+\infty} \Phi_{ln}(\mathbf{k}) dk_2 dk_3. \quad (6)$$

Up to this point we were concerned with an ideal measuring instrument i.e., one without dimensions. In analyzing the results of a real instrument we can use the same quantities as defined above, but now for the measured values. To indicate this, we will add an index m, so $u_l^{(m)}$ is the signal induced in component l by the wind vector $\mathbf{u}$. In this way, we will also use $U_l^{(m)}$, $\Phi_{ln}^{(m)}$ and $F_{ln}^{(m)}$. The equations for the indexed quantities will not all be given anew, but they will be indicated by adding an m to the number of the corresponding equation for an ideal sensor. What we wish to find in this article is a relation between (6) and its counterpart

$$F_{ln}^{(m)}(k_1) = \iint_{-\infty}^{+\infty} \Phi_{ln}^{(m)}(\mathbf{k}) dk_2 dk_3. \quad (6m)$$

To this end, we will discuss the nature of the measured signals to establish a relation between $\Phi_{ln}^{(m)}$ and Φ_{ln} for the deviations of types 2 and 3, as mentioned in the foregoing paragraph, then we will perform the integrations to obtain the desired result, using (3).

3. Application to the PA

The signal of a ring is considered to be the sum of the signals from the eight individual sensor openings (cf Section 1). For reasons of normalization, the mean is taken instead of the sum; this has no influence on the argument. So, using (1) and neglecting (as stated) the dimensions of the openings of a ring,

$$u_l^{(m)}(\mathbf{x}) = \frac{1}{8} \sum_{j=1}^{8} u_l(\mathbf{x} + \mathbf{r}_j) = \frac{1}{8} \sum_{j=1}^{8} \int_{-\infty}^{+\infty} \exp\{i\mathbf{k} \cdot (\mathbf{x} + \mathbf{r}_j)\} dU_l(\mathbf{k}), \quad (7)$$

where $\mathbf{x}$ denotes the center of the ring and the $\mathbf{r}_j$ are the position vectors of the sensor openings relative to this center. We suppose the sensors to have a cosine directional dependence i.e., to be sensitive only to the wind component along its axis. This assumption is permitted because the first step in the interpretation of data is a transformation from measured signals to wind components using calibration data (Oost, 1983). Comparing ($1m$) and (7) it follows that

$$dU_l^{(m)}(\mathbf{k}) = \frac{1}{8} \sum_{j=1}^{8} \exp(i\mathbf{k} \cdot \mathbf{r}_j) dU_l(\mathbf{k}),$$

from which with (2) and ($2m$)

$$\Phi_{ln}^{(m)}(\mathbf{k}) = \frac{1}{64} \sum_{h,j=1}^{8} \exp[i\mathbf{k} \cdot (\mathbf{r}_j - \mathbf{r}_h)] \Phi_{ln}(\mathbf{k}),$$

and finally ($6m$) becomes

$$F_{ln}^{(m)}(k_1) = \frac{1}{64} \iint_{-\infty}^{+\infty} \sum_{h,j=1}^{8} \exp\{i\mathbf{k} \cdot (\mathbf{r}_j - \mathbf{r}_h)\} \Phi_{ln}(\mathbf{k}) dk_2 dk_3. \quad (8)$$

To calculate the effect of the distance between the centers of the components, we use again the cosine direction dependence of the rings.

The mutually orthogonal components of the instrument have their centers in P_1, P_2 and P_3 (Fig. 1), and they are sensitive to respectively, the x, y and z components of the wind.

The wind has its own coordinate system, with components u_1, along the mean wind direction, u_2 perpendicular to u_1 and parallel to the xy-plane and u_3, perpendicular to u_1 and u_2. For greater clarity we will leave the effect just treated, due to the distance of the sensor openings along a ring, out of our formulae, until after the treatment of the effect now under consideration.

The signals of the rings can be written as linear combinations of the three windcomponents at P_1, P_2 and P_3 such that

$$\left.\begin{aligned} u_x^{P_1} &= a_{11}u_1^{P_1} + a_{12}u_2^{P_1} + a_{13}u_3^{P_1} \\ u_y^{P_2} &= a_{21}u_1^{P_2} + a_{22}u_2^{P_2} + a_{23}u_3^{P_2} \\ u_z^{P_3} &= a_{31}u_1^{P_3} + a_{23}u_2^{P_3} + a_{33}u_3^{P_3} \end{aligned}\right\}, \quad (9)$$

where $u_i^{P_j}$ denotes the windcomponent in the i-direction at P_j; The a_{ij} are coefficients which depend only on the wind direction. The matrix $\mathbf{A}$ of the coefficients a_{ij} represents a rotation of the coordinate system. It is therefore an orthogonal matrix. The inverse transformation is given by

$$\left.\begin{aligned} u_1^{P_1} &= c_{11}u_x^{P_1} + c_{12}u_y^{P_1} + c_{13}u_z^{P_1} \\ u_2^{P_2} &= c_{21}u_x^{P_2} + c_{22}u_y^{P_2} + c_{23}u_z^{P_2} \\ u_3^{P_3} &= c_{31}u_x^{P_3} + c_{23}u_y^{P_3} + c_{33}u_z^{P_3} \end{aligned}\right\}. \quad (10)$$

Because of the orthogonality,

$$a_{jn} = c_{nj}. \tag{11}$$

The PA measures $u_x^{P_1}$, $u_y^{P_2}$ and $u_z^{P_3}$. The usual estimate for (u_1, u_2, u_3)—the wind vector in the center of the sensor system—is obtained by neglecting the distance between the components. For the measured wind vector this gives

$$\left.\begin{aligned} u_1^{(m)} &= c_{11}u_x^{P_1} + c_{12}u_y^{P_2} + c_{13}u_z^{P_3} \\ u_2^{(m)} &= c_{21}u_x^{P_1} + c_{22}u_y^{P_2} + c_{23}u_z^{P_3} \\ u_3^{(m)} &= c_{31}u_x^{P_1} + c_{23}u_y^{P_2} + c_{33}u_z^{P_3} \end{aligned}\right\}. \tag{12}$$

Combining (12) and (10) we obtain

$$u_j^{(m)} = c_{jn}a_{nl}u_l^{P_n} \quad j, l, n = 1, 2, 3, \tag{13}$$

where a summation over repeated indices is understood.

The (x, y, z)-system can be transformed into the (1, 2, 3)-system by a rotation over an angle α in the xy-plane (the angle between MB and the x-axis in Fig. 1) and angle ζ in the plane through MB and the z-axis (for which we have chosen the angle between the $-u_1$ direction and MB), because both systems are orthogonal. The transformation coefficients are a_{ij} and c_{ij}, so

$$\left.\begin{aligned} a_{11} &= c_{11} = \cos\zeta\cos\alpha & a_{12} &= c_{21} = -\sin\alpha \\ a_{13} &= c_{31} = -\sin\zeta\cos\alpha & a_{21} &= c_{12} = \cos\zeta\sin\alpha \\ a_{22} &= c_{22} = \cos\alpha & a_{23} &= c_{32} = -\sin\zeta\sin\alpha \\ a_{31} &= c_{13} = \sin\zeta & a_{32} &= c_{23} = 0 \\ a_{33} &= c_{33} = \cos\zeta \end{aligned}\right\}. \tag{14}$$

Combining (7) and (13) we find for the combination of both effects

$$u_j^{(m)} = c_{jn}a_{nl}\frac{1}{8}\sum_{h=1}^{8} u_l(\mathbf{P}_n + \mathbf{r}_h)$$

$$= \frac{1}{8}c_{jn}a_{nl}\sum_{h=1}^{8}\int_{-\infty}^{+\infty}\exp[ik\cdot(\mathbf{P}_n + \mathbf{r}_h)]dU_l(\mathbf{k}),$$

resulting in the same way as with Eq. (8) in

$$F_{lj}^{(m)}(k_1) = \frac{1}{64}c_{lq}a_{qn}c_{js}a_{sp}\iint_{-\infty}^{+\infty}\exp[i\mathbf{k}\cdot(\mathbf{P}_q - \mathbf{P}_s)]$$

$$\times[\sum_{t=1}^{8}\exp(i\mathbf{k}\cdot\mathbf{r}_{qt})][\sum_{t=1}^{8}\exp - (i\mathbf{k}\cdot\mathbf{r}_{st})]$$

$$\times\Phi_{np}dk_2dk_3 \quad (j, l, n, p, q, s = 1, 2, 3) \tag{15}$$

Vector $\mathbf{r}$ has two indices now, the first one denoting the component (ring) and the second one its position in the ring. Using (3), (15) can be calculated. What we wish to know, however, is not (15) itself, but the ratio of (15) and the spectrum measured by a point sensor, as given by (6). The ratio of (15) and (6), which is 1 for large wavelengths, will be indicated, following Kaimal *et al.*, as the transfer function (TF).

4. Calculations

We will calculate the TF for the u_1, u_2 and u_3 autospectra; this means that in (15) $l = j$[in (6): $l = n$] and $l = 1, 2, 3$. The calculation is performed using (3); with this type of spectrum, (6) can be evaluated analytically.

This is not the case with (15). Originally the double integrals were calculated using straightforward numerical integration. Due to the oscillating functions in (15) a small step size was required, resulting in long computing times: the calculation of $F_{11}^{(m)}$, $F_{22}^{(m)}$ and $F_{33}^{(m)}$ for one value of k_1 required a minimum of 1300 sec CPU-time on a Burroughs B6800 computer, despite the use of a fairly fast Gaussian integration algorithm. However, (15) can be rewritten as

$$F_{lj}^{(m)}(k_1) = \frac{\epsilon^{2/3}}{4\pi}\sum_{\substack{q,n,s\\p,\kappa,\lambda}} c_{lq}c_{nq}c_{js}c_{ps}$$

$$\times\exp(-ik_1B_1)\times\iint_{-\infty}^{+\infty}\exp(-ik_2B_2 - ik_3B_3)$$

$$\times\frac{(k_1^2 + k_{23}^2)\delta_{np} - k_nk_p}{(k_1^2 + k_{23}^2)^{\gamma}}dk_2dk_3$$

$$j, l, n, p, q, s, = 1, 2, 3; \quad \kappa, \lambda = 1, 2, \ldots, 8, \tag{16}$$

using (3) and (11) and the notation

$$B_j = (B_{qs\kappa\lambda})_j = (P_s - P_q + r_{s\lambda} - r_{q\kappa})_j;$$

$$k_{23}^2 = k_2^2 + k_3^2; \quad \gamma = 17/6.$$

All summations have been indicated at the sigma sign for greater clarity. Using the substitutions

$$\left.\begin{aligned} k_2 &= k_{23}\cos\theta, \quad k_3 = k_{23}\sin\theta \\ B_2 &= R\cos\phi, \quad B_3 = R\sin\phi \end{aligned}\right\},$$

Eq. (16) can be transformed into

$$F_{lj}^{(m)}(k_1) = \frac{\epsilon^{2/3}}{144\pi}\sum_{\substack{q,n,s\\p,\kappa,\lambda}} c_{lq}c_{nq}c_{js}c_{ps}\exp(-ik_1B_1)$$

$$\times\left[\left(k_1^2 - \frac{1}{R}\frac{\partial}{\partial R} - \frac{\partial^2}{\partial R^2} - \frac{1}{R^2}\frac{\partial^2}{\partial\phi^2}\right)\delta_{np} - D_nD_p\right]$$

$$\times\int_0^{\infty}\frac{k_{23}dk_{23}}{(k_1^2 + k_{23}^2)^{\gamma}}\int_{-\pi}^{+\pi}\exp[-ik_{23}R\cos(\theta - \phi)]d\theta, \tag{17}$$

with

$$D_1 = -k_1; \quad D_2 = -i\left(\cos\phi \frac{\partial}{\partial R} - \frac{\sin\phi}{R}\frac{\partial}{\partial \phi}\right);$$

$$D_3 = -i\left(\sin\phi \frac{\partial}{\partial R} + \frac{\cos\phi}{R}\frac{\partial}{\partial \phi}\right).$$

The second integration is of a standard type and produces a zero order Bessel function of the first kind (J_0). Substituting this, the form of the remaining integral is

$$\int_0^\infty 2\pi J_0(k_{23}R)\frac{k_{23}dk_{23}}{(k_1^2 + k_{23}^2)^\gamma},$$

which is again a standard form (Gradshteyn and Ryzhik, 1965), resulting in a Hankel-function with imaginary argument (K-function). The result, substituting $\rho = k_1 r$, is

$$F_{lj}^{(m)}(k_1) = \frac{\epsilon^{2/3}k_1^{-5/2}2^{1/6}}{288\Gamma(17/6)} \sum_{\substack{q,n,s \\ p,\kappa,\lambda}} c_{lq}c_{nq}c_{js}c_{ps}\exp(-ik_1B_1) \times \left[\left(1 - \frac{\partial^2}{\partial\rho^2} - \frac{1}{\rho}\frac{\partial}{\partial\rho} - \frac{1}{\rho^2}\frac{\partial^2}{\partial\phi^2}\right)\delta_{np} - D_nD_p\right] \times \rho^{11/6}K_{11/6}(\rho), \quad (18)$$

with

$$D_1 = -1, \quad D_2 = -i\left(\cos\phi \frac{\partial}{\partial\rho} - \frac{\sin\phi}{\rho}\frac{\partial}{\partial\phi}\right),$$

$$D_3 = -i\left(\sin\phi \frac{\partial}{\partial\rho} + \frac{\cos\phi}{\rho}\frac{\partial}{\partial\phi}\right),$$

and Γ the gamma function.

The derivatives of the K-function are also known from literature (Abramowitz and Stegun, 1964) and our final result is, using the summation convention again,

$$F_{lj}^{(m)}(k_1) = \frac{\epsilon^{2/3}k_1^{-5/3}2^{1/6}}{512\Gamma(17/6)} c_{lq}c_{nq}c_{js}c_{ps}Q_{np} \times \sum_{\kappa,\lambda=1}^{8}\exp(-ik_1B_1),$$

$$j, l, q, n, s, p = 1, 2, 3. \quad (19)$$

$$\left.\begin{aligned} Q_{11} &= \rho^{5/6}[2K_{5/6}(\rho) - \rho K_{1/6}(\rho)] \\ Q_{12} &= Q_{21} = -i\cos\phi\rho^{11/6}K_{5/6}(\rho) \\ Q_{13} &= Q_{31} = -i\sin\phi\rho^{11/6}K_{5/6}(\rho) \\ Q_{22} &= {}^8/_3\rho^{5/6}K_{5/6}(\rho) + \rho^{11/6}\cos^2\phi K_{1/6}(\rho) \\ Q_{23} &= Q_{32} = \cos\phi\sin\phi\rho^{11/6}K_{1/6}(\rho) \\ Q_{33} &= {}^8/_3\rho^{5/6}K_{5/6}(\rho) + \rho^{11/6}\sin^2\phi K_{1/6}(\rho) \end{aligned}\right\}.$$

$$\Gamma(17/6) = 1.72453$$

The calculation of the K-functions can be done once and for all, after which the time needed for the calculation is reduced to a small fraction of the original value: the calculation, mentioned earlier in this section now took about 4 seconds on the same B6800. The slow program could nevertheless be put to good use in the debugging phase, as it will be evident that both programs should yield the same values.

The results of our calculations are given in a number of figures which show the effect of the variation of several parameters on the TF. In Fig. 2, the meaning of azimuth and elevation as used in the remaining figures is shown. The lines in Figs. 3–7 have been drawn using third-order spline functions to interpolate between the calculated values.

Figures 3a and 3b show the effect of an elevation and an azimuth variation respectively on the TF of fluctuations in the k_1 direction (along the mean wind). Figs. 4a and 4b show the same for the k_2 and Figs. 5a and 5b for the k_3 direction. The most striking features in these figures are the positive and negative resonance type deviations at $\sim$0.016 mm^{-1}. Kaimal *et al.* (1968) also found a comparable deviation for the k_1 – TF of their sonic anemometer and a slight depression for the k_2 – *TF*. The maximum effect of path separation on k_1 is larger with the sonic than with the PA; whereas Kaimal *et al.* calculate a maximum value of 2.5 for the deviation for a 120° array the PA has a maximum of 1.4 for an infinite ratio of component separation and ring dimensions. Like the sonic, the PA has an optimum value where the TF deviates only slightly from 1 for a maximum range of wavenumbers: this is the case when the distance between the rings is about 3 times their radius (the dashed curve in Fig. 6). It must be kept in mind, however, that the intrinsic frequency response, mentioned in the introduction, has not been taken into account. This frequency response

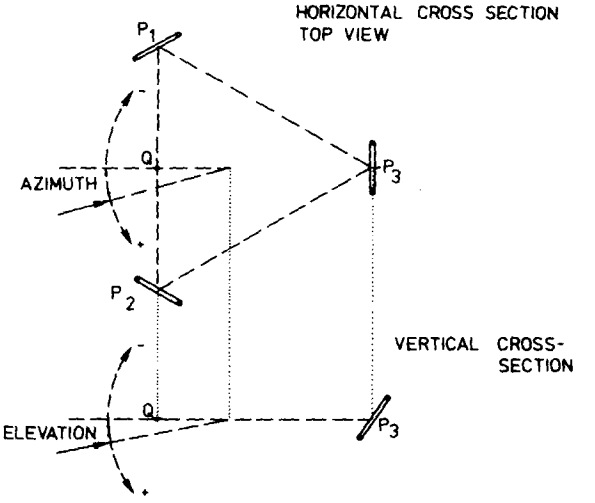

FIG. 2. Elevation and azimuth. The solid arrows indicate the projections of the wind vector.

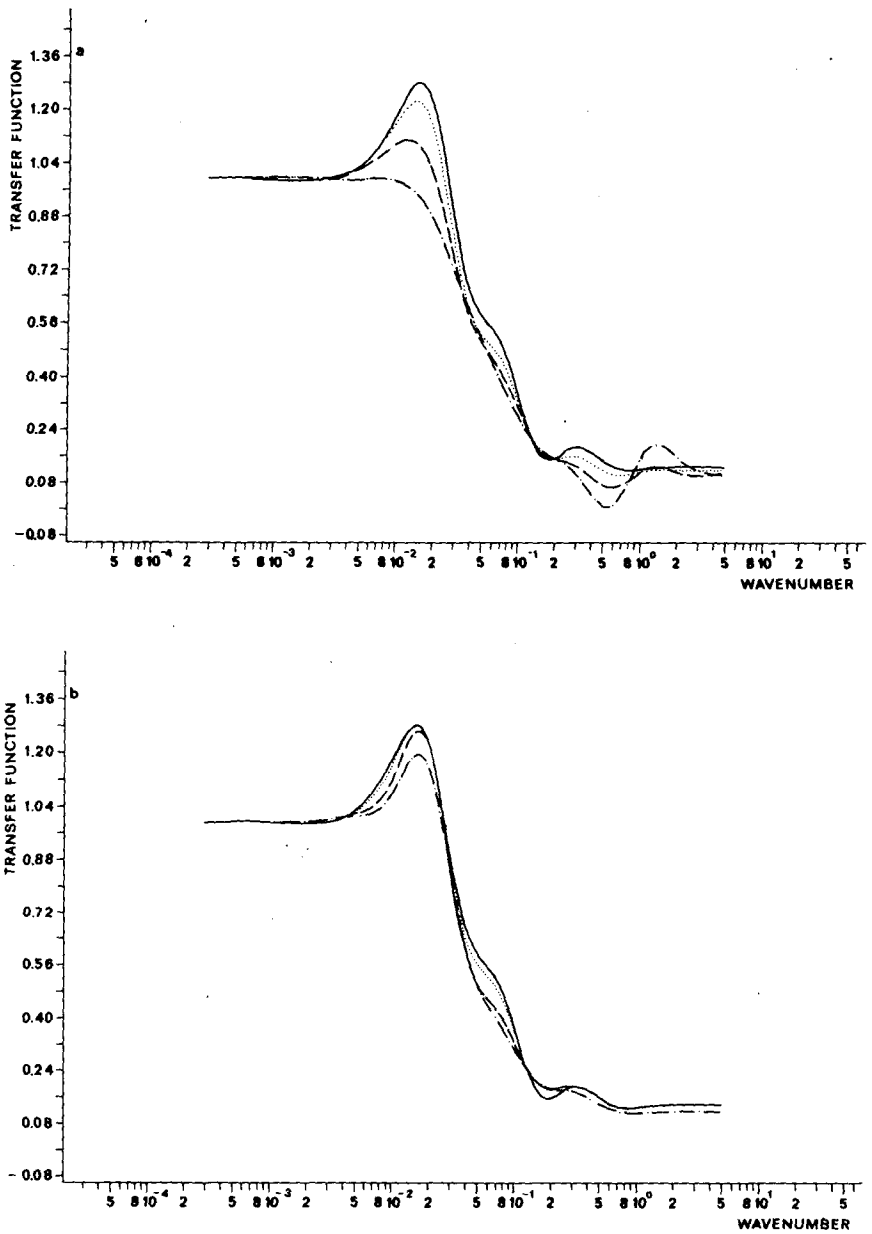

FIG. 3. Transfer function (ratio of the available and detected one-dimensional spectral densities) in the u_1-direction as function of elevation and azimuth for an inertial subrange type of spectrum. The wavenumber k is in mm^{-1}. Ring diameter is 30 mm. Distance between ring centers is 150 mm. (a) Azimuth = 0 and elevation 0° (solid), 10° (dotted), 20° (dashed) and 30° (dash-dotted). (b) Elevation = 0° and azimuth 0° (solid), 10° (dotted), 20° (dashed), 30° (dash-dotted).

has a negative slope in the range corresponding to the place of the maximum in Fig. 3, which has a compensating effect on the TF.

The strength of the maximum changes quite strongly with the elevation but is hardly influenced by changes in the azimuth. The highest maximum occurs at an elevation of 0°; the effects are more or less symmetric around this elevation angle, at least for an azimuth angle of 0°.

The effect of enlarging the ratio of the distance between the ring centers and the ring diameter is shown in Fig. 6. When the centers of the rings coincide, the TF curve has the appearance of a low-pass filter with a low steepness (about 1.3 dB/octave at the 3 dB point). When the rings are placed at larger mutual distances a "hump" appears, which grows to the maximum of Fig. 3 (the same type of behavior appears with the k_2 and k_3 TF).

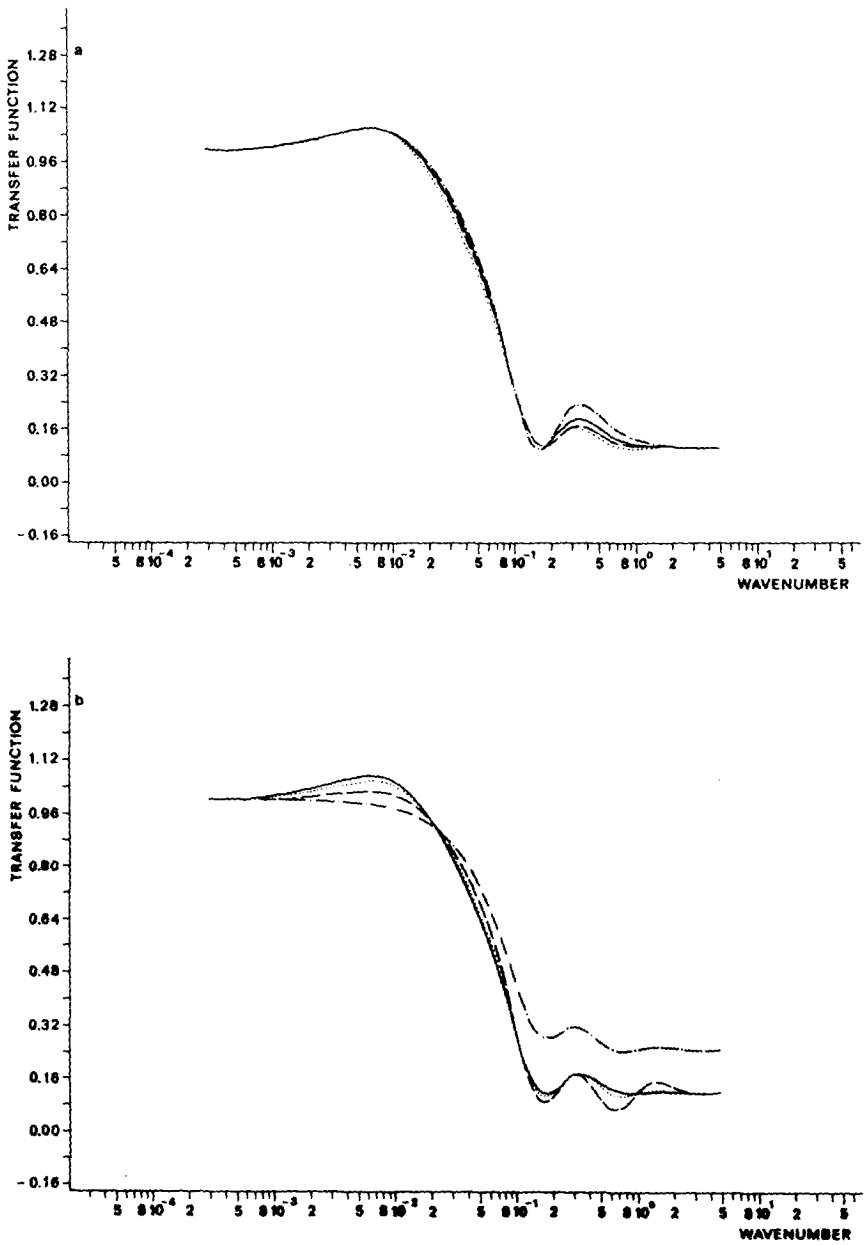

FIG. 4. As in Fig. 3, but for the u_2-direction.

We have also checked the sensitivity of the results to the shape of the velocity spectrum. These tests showed the height of the maxima and minima to be proportional to the exponent in Eq. (3) for values in the range of $-\frac{4}{3}$ to -2. Finally, Fig. 7 gives the k_1 – TF for a ring diameter 0.

Comparing Figs. 3a and 7 it is clear that the use of a finite ring smoothes the high-frequency drop-off and gives a lower high-frequency tail. This may be considered as one of the causes of the well-behaving angular response of the PA at higher frequencies. In all figures, the transfer function finally falls off to a value which is different from 0, due to the neglect of the dimensions of the sensor openings.

5. Conclusions

The change in the response of the pressure anemometer with wavelength has been calculated and presented in a number of figures which give the transfer function as defined by Kaimal *et al.* (1968).

From these figures it can be concluded that the 3 dB point will lie at a wavelength about equal to the distance between the ring centers. Before the final drop-

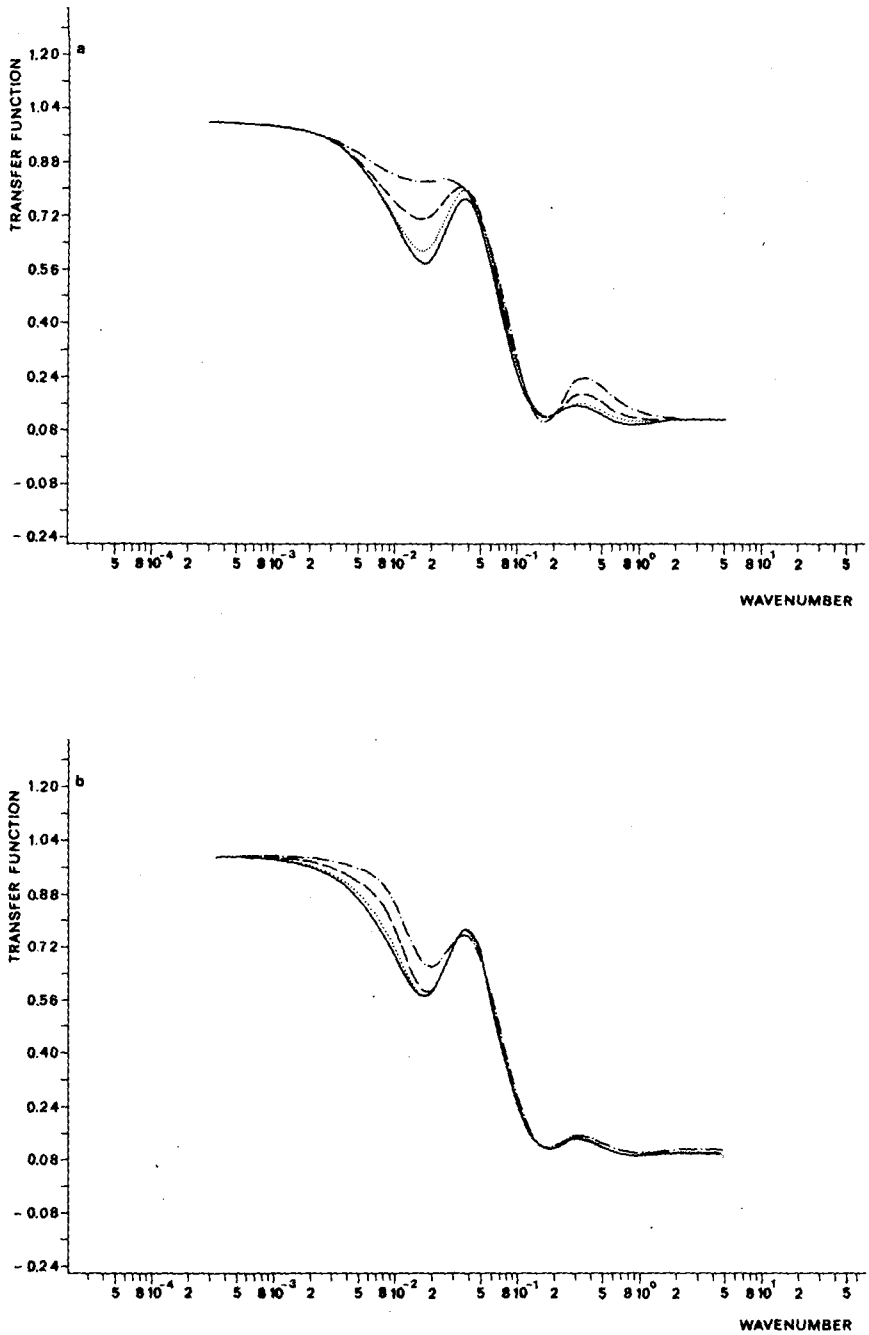

FIG. 5. As in Fig. 3, but for the u_3-direction.

off in these figures, there is a maximum, which becomes more pronounced as the ratio of the ring diameter and the distance between the ring centers diminishes. This maximum can be sufficiently pronounced to be taken into account when interpreting data.

However, the calculations in this article are not the full story: the pressure anemometer also has an intrinsic frequency response, as mentioned in the introduction. A few experimental results indicate that this frequency response starts falling off at a wavelength between 1 and 0.4 m, depending on the wind speed. The effects of the combination of the intrinsic response with the transfer function, calculated in this article, is a leveling of the maximum and a steepening of the final intensity drop; the 3 dB point will not shift very much.

It may safely be concluded that the instrument gives

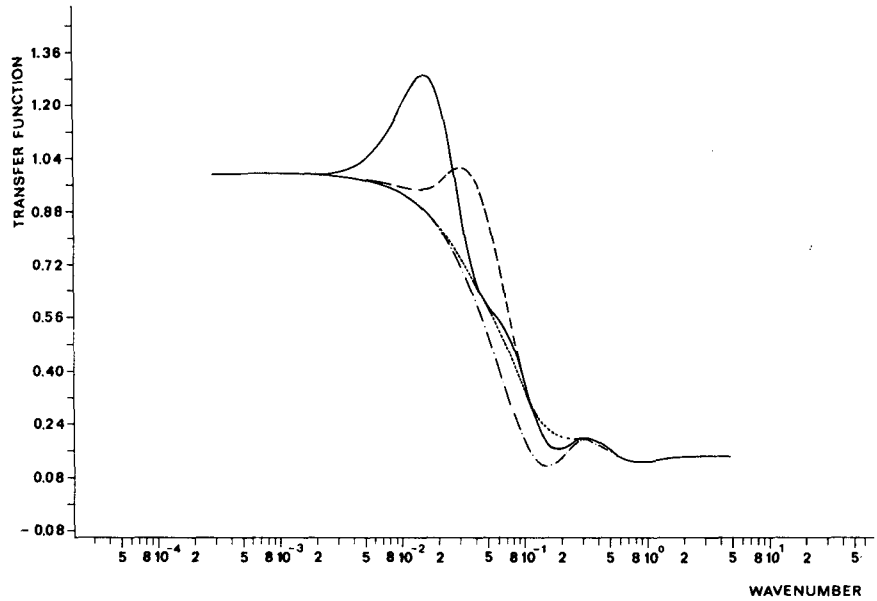

FIG. 6. Transfer function in the u_1-direction as function of the distance between the rings. Azimuth 0°, elevation 0° and ring diameter 30 mm. Distance between ring centers: 0 (dash-dotted), 15 (dotted), 50 (dashed) and 150 mm (solid).

useful data for frequencies up to 25 Hz, corresponding to wavenumbers of 0.04 mm^{-1} at 4 m s^{-1} and 0.01 mm^{-1} at 16 m s^{-1}, provided corrections are made for the maximum in the transfer function, especially at low wind velocities.

This conclusion is not contradicted by our field results, which were obtained at a research platform off the Dutch coast. At the end of the high-frequency end of the $f^{-5/3}$ slope in our spectra, a small hump was present before the final drop-off. However, the devia-

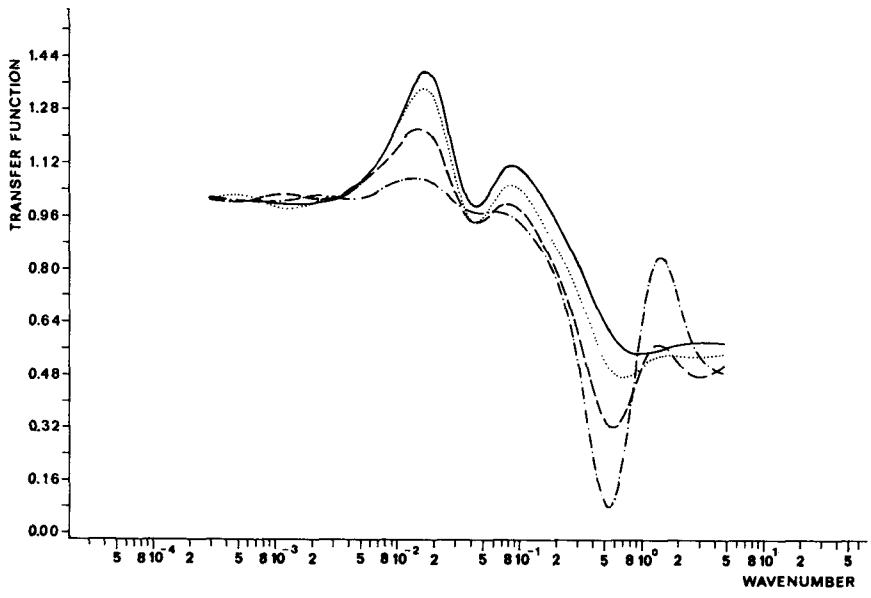

FIG. 7. Transfer function in the u_1-direction as function of elevation at a ring diameter 0. Distance between ring centers 150 mm and azimuth 0°. Elevation 0° (solid), 10° (dotted), 20° (dashed) and 30° (dash-dotted).

tions were too small compared to the variability of the spectrum to permit a detailed comparison.

REFERENCES

Abramowitz, M., and I. A. Stegun, 1964: *Handbook of Mathematical Functions.* U.S. Department of Commerce, 1046 pp.

Fox, L. H., 1968: Continuous-wave three-component sonic anemometer. Final Report, AFCRL-68-0180, Bolt, Beranek and Newman Inc., 57 pp.

Gradshteyn, I. S., and I. M. Ryzhik, 1965: *Table of Integrals, Series and Products.* Academic Press, 1086 pp.

Gurvich, A. S., 1962: The pulsation spectra of the vertical component of wind velocity and their relations to the micrometeorological conditions. *Izv. Acad. Sci. USSR Atmos. Oceanic Phys.*, **4**, 101–136.

Horst, Th.W., 1973: Spectral transfer functions for a three component sonic anemometer. *J. Appl. Meteor.*, **12**, 1072–1075.

Kaimal, J. J., J. C. Wyngaard and D. A. Haugen, 1968: Deriving power spectra from a three component sonic anemometer. *J. Appl. Meteor.*, **7**, 827–837.

Lumley, J. L., and H. A. Panofsky, 1964: *The Structure of Atmospheric Turbulence.* Wiley and Sons, 239 pp.

Oost, W. A., 1983: The pressure anemometer—an instrument for adverse circumstances. *J. Climate Appl. Meteor.*, **22**, 2075–2084.

Silverman, B. A., 1968: The effect of spatial averaging on spectrum estimation. *J. Appl. Meteor.*, **7**, 168–172.

Uberoi, M. S., and L. S. G. Kovasznay, 1953: On mapping and measurement of random fields. *Quart. Appl. Math.*, **10**, 375–393.